Supporting Information

Nonvolatile Organic Field-Effect Transistor Memory from Pyrene-fused Azaindacene Regioisomers

Duan-Wu Liu,[a] Yamin Zhang,*[a] Xiang-Yang Li,[a] Qi Xiao,[a] Wen-Jing Sun,[a] Xiangfeng Shao,[a] and Hao-Li Zhang*[a]

[a.] D. W. Liu, Y. M. Zhang, X. Y. Li, Q. Xiao, W. J. Sun, Prof. X. F. Shao, Prof. H. L. Zhang
State Key Laboratory of Applied Organic Chemistry, Key Laboratory of Special Function Materials and Structure Design, College of Chemistry and Chemical Engineering, Lanzhou University, Lanzhou 730000, P. R. China,

[b.] Prof. H. L. Zhang
Tianjin Key Laboratory of Molecular Optoelectronic Sciences, Department of Chemistry, Tianjin University, Collaborative Innovation Center of Chemical Science and Engineering (Tianjin), Tianjin 300072, P. R. China

***Corresponding Authors:**

Hao-Li Zhang E-mail: haoli.zhang@lzu.edu.cn

Yamin Zhang E-mail: zym@lzu.edu.cn

1. Synthesis Steps

The 2,7-di-tert-butylpyrene (1) and 2,7-di-tert-butylpyrene-4,5-dione (2) are synthesized by the literature method.[39]

9,10-dibromo-2,7-di-tert-butylpyrene-4,5-dione (3). Compound 2 (1 g, 3 mmol) and N-Bromosuccinimide (2.1 g, 12 mmol) were dissolved in H_2SO_4 (4 mL), and start stirring. Then, the reaction mixture was stirred at room temperature for 4h. The mixed solution was poured into water and filtered to obtain the compound 3 (873 mg). Brown solid, 58% yield. **^{1}H NMR (400 MHz, $CDCl_3$)** δ 8.66 (d, J=2.0 Hz, 2H), 8.55 (d, J=2.0 Hz, 2H), 1.50 (s, 18H). **^{13}C NMR (101 MHz, $CDCl_3$)** δ 179.79 (s), 152.56 (s), 132.92 (s), 131.07 (s), 129.56 (s), 129.44 (s), 126.60 (s), 126.19 (s), 35.52 (s), 31.08 (s).

4,5-dibromo-2,7-di-tert-butyl-9,10-bis(hexyloxy)pyrene (4). Compound 3 (2 g, 4 mmol), tetrabutylammonium bromide (428 mg, 1.3 mmol) and $Na_2S_2O_4$ (3.5 g, 20 mmol) were added in a mixture solution of THF/water (1:1, 100 mL). After stirring at room temperature for 5 minutes, a solution of KOH (2.2 g, 40 mmol) in H_2O (60 mL) was added to the reaction mixture followed by 1-bromohexane (3.28 g, 20 mmol). Then, the reaction mixture was stirred at 100°C for 4 h. The reaction mixture was cooled and the crude was extracted with ethyl acetate (2 × 20 mL). The organic phase was washed with salt water and dried by anhydrous magnesium sulfate. The solvent was removed under reduced pressure. The crude product was purified by column chromatography (PE as eluent) to provide compound 4 (1.91 g). Colorless solution, 71% yield. **^{1}H NMR (400 MHz, $CDCl_3$)** δ 8.70 (d, J=1.6 Hz, 2H), 8.64 (d, J=1.6 Hz, 2H), 4.35

(t, J=6.4 Hz, 4H), 2.04-1.90 (m, 4H), 1.71-1.60 (m, 22H), 1.45-1.38 (m, 8H), 0.95 (t, J=6.9 Hz, 6H). **^{13}C NMR (101 MHz, $CDCl_3$)** δ 150.11 (s), 143.97 (s), 130.21 (s), 128.65 (s), 126.90 (s), 123.67 (s), 120.67 (s), 118.34 (s), 74.00 (s), 35.84 (s), 32.02 (d, J=11.3 Hz), 30.80 (s), 26.43 (s), 22.87 (s), 14.22 (s).

2,7-di-tert-butyl-9,10-bis(hexyloxy)pyrene-4,5-dicarbonitrile (5). Compound 4 (670 mg, 1 mmol), CuCN (352 mg, 4 mmol) were added in anhydrous NMP (100 mL). The mixture was stirred at 180 °C for 6 hours under a nitrogen atmosphere. Then, the solvent was removed and cooled. An excess of ammonia was added to the flask and stirred overnight at room temperature. The precipitate was filtered and the filtrate was extracted with ethyl acetate (3×100 mL). The combined organic phase was washed with brine, dried over anhydrous magnesium sulfate, and concentrated. The crude product was purified by column chromatography (PE:CH_2Cl_2=4:1) to provide compound 5. Yellow solid (242 mg), 43% yield. **^{1}H NMR (400 MHz, $CDCl_3$)** δ 8.79 (d, J=1.7 Hz, 2H), 8.58 (d, J=1.7 Hz, 2H), 4.36 (t, J=6.5 Hz, 4H), 2.03–1.90 (m, 4H), 1.69–1.61 (m, 22H), 1.45-1.36 (m, 8H), 0.94 (t, J=7.1 Hz, 6H). **^{13}C NMR (101 MHz, $CDCl_3$)** δ 151.51 (s), 144.28 (s), 129.15 (s), 126.70 (s), 121.55 (s), 121.22 (s), 120.95 (s), 117.21 (s), 115.62 (s), 77.48 (s), 77.16 (s), 76.84 (s), 74.11 (s), 35.97 (s), 31.91 (s), 30.73 (s), 26.39 (s), 22.85 (s), 14.20 (s).

2,7-di-tert-butyl-9,10-bis(hexyloxy)pyrene-4,5-dicarboxylic acid (6). Compound 5 (564 mg, 1 mmol) and KOH (275 mg, 5 mmol) were added into a mixture solution of ethanol/water (1:1, 50 mL) in a 100 mL round-bottom flask and heated to reflux with stirring overnight. After

cooling down, the reaction mixture was acidified to pH=1 with concentrated hydrochloric acid and the solution was filtered. The crude product was purified by column chromatography (PE:CH_2Cl_2=1:1) to provide compound 6. Orange solid (469 mg), 78% yield. **^{1}H NMR (400 MHz, $CDCl_3$)** δ 9.21 (d, J=1.5 Hz, 2H), 8.81 (d, J=1.5 Hz, 2H), 4.37 (t, J=6.4 Hz, 4H), 2.03-1.89 (m, 4H), 1.79-1.56 (m, 22H), 1.51-1.33 (m, 8H), 0.94 (t, J=6.9 Hz, 6H). **^{13}C NMR (101 MHz, $CDCl_3$)** δ 164.43 (s), 151.73 (s), 144.44 (s), 129.46 (s), 129.32 (s), 124.17 (s), 123.76 (s), 121.57 (s), 120.61 (s), 74.28 (s), 36.17 (s), 32.15 (s), 30.98 (s), 26.62 (s), 23.06 (s), 14.41 (s).

***syn*-B2IPIO and *anti*-B2IPIO.** 1,2,4,5-benzenetetramine tetrahydrochloride (85 mg, 0.3 mmol) and compound 6 (300 mg, 0.5 mmol) were added in pyridine (5 mL). The mixture was heated to 110 °C with stirring under the nitrogen atmosphere for one night. The solvent was removed by suction filtration, and the solid residue was the syn-anti isomerized crude product. The isomers can be separated by column chromatography (PE:CH_2Cl_2=4:1). ***syn*-B2IPIO** (61.5 mg), red solid, 39% yield. **^{1}H NMR (400 MHz, $CDCl_3$)** δ 9.31 (d, J=1.7 Hz, 2H), 9.24 (s, 2H), 8.74 (d, J=1.2 Hz, 2H), 8.62 (d, J=1.7 Hz, 2H), 8.06 (d, J=6.0 Hz, 2H), 4.25 (t, J=6.3 Hz, 4H), 4.18 (t, J=6.3 Hz, 4H), 1.97-1.81 (m, 8H), 1.74 (s, 18H), 1.69-1.61 (m, 26H), 1.39 (dt, J=7.3, 5.4 Hz, 16H), 0.94 (td, J=6.9, 2.4 Hz, 12H). **^{13}C NMR (101 MHz, $CDCl_3$)** δ 161.99 (s), 157.79 (s), 150.79 (s), 150.60 (s), 147.38 (s), 144.03 (s), 143.77 (s), 131.96 (s), 129.21 (s), 128.72–128.38 (m), 125.79 (s), 123.44 (s), 123.18 (s), 122.17 (s), 120.75 (s), 120.50 (s), 118.74 (d, J=10.5 Hz), 114.45 (s), 95.59 (s), 73.53 (d, J=9.1 Hz), 35.80 (s), 31.96 (d, J=7.9 Hz), 31.80 (d, J=1.9 Hz), 30.59 (d, J=5.3 Hz), 26.28 (d, J=2.5 Hz), 22.70 (d, J=2.0 Hz), 14.08 (s). **ESI-HRMS**

calculated for $C_{82}H_{98}O_6N_4$([M+H]$^+$): 1235.7559; Found 1235.7346. $C_{82}H_{98}O_6N_4$([M+Na]$^+$): 1257.7379; Found 1235.7346.

***anti*-B2IPIO** (15.4 mg), black-red solid, 10% yield. **^{1}H NMR (600 MHz, $CDCl_3$)** δ 9.36 (s, 2H), 9.32 (s, 2H), 8.77 (s, 2H), 8.67 (s, 2H), 8.18 (s, 2H), δ 4.34 (dd, *J*=13.8, 6.7 Hz, 8H), 1.98 (dd, J=13.9, 7.3 Hz, 8H), 1.76–1.71 (m, 18H), 1.70–1.61 (m, 26H), 1.46–1.36 (m, 16H), 0.99–0.91 (m, 12H). **^{13}C NMR** cannot be obtained due to the extremely poor solubility. **ESI-HRMS** calculated for $C_{82}H_{98}O_6N_4$([M+H]$^+$): 1235.7559; Found 1235.7769. $C_{82}H_{98}O_6N_4$([M+Na]$^+$): 1257.7379; Found 1257.7438.

It is worth noting that the proton peaks of core benzene are clearly different for the *syn*-B2IPIO and *anti*-B2IPIO. The *anti*-B2IPIO shows a single peak, while the *syn*-B2IPIO shows two single peaks with slightly different chemical shifts.

2. Spectroscopic Properties

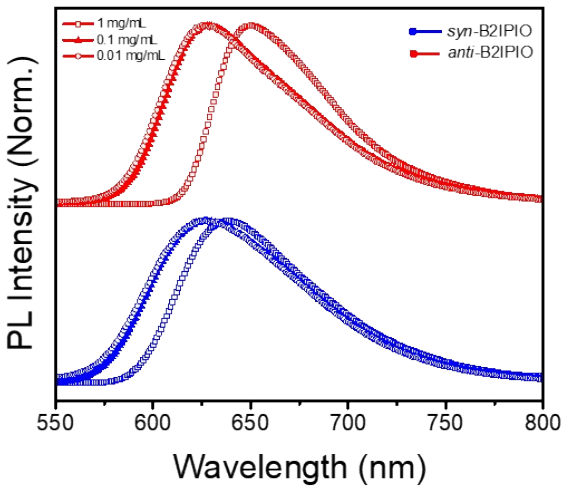

Figure S1. PL spectra of *syn*-B2IPIO and *anti*-B2IPIO in trichloromethane solution at various concentrations: 0.01 mg mL^{-1}, 0.1 mg mL^{-1}, and 1 mg mL^{-1}.

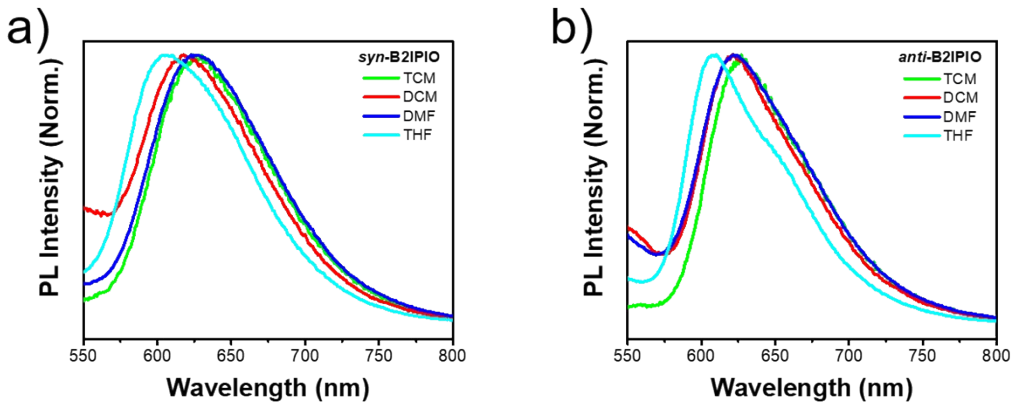

Figure S2. The PL spectra of the a) *syn*-B2IPIO and b) *anti*-B2IPIO in different solutions (DCM, TCM, DMF and THF).

Table. S1 Photophysical, thermal, and electrochemical properties of *syn*-B2IPIO and *anti*-B2IPIO.

Molecule	T_d [°C]	$\lambda_{abs,\ max/nm}$		$\lambda_{PL,\ max/nm}$		E_g^{opt} [eV]	E_g^{opt} [eV]	E_{HOMO} [eV]	E_{LUMO} [eV]
		Solution	Film	Solution	Film				
syn-B2IPIO	353	306	344	625	659	2.08	2.29	-5.66	-3.37
anti-B2IPIO	356	310	345	625	668	2.00	2.35	-5.62	-3.27

Table S2. Comparison of the Dipole Moments (in D) of *syn*-B2IPIO and *anti*-B2IPIO.

	X	*Y*	*Z*	total
syn-B2IPIO	0.0201	-1.6450	0.0078	1.6452
anti-B2IPIO	0	0	0	0

3. Cyclic voltammograms

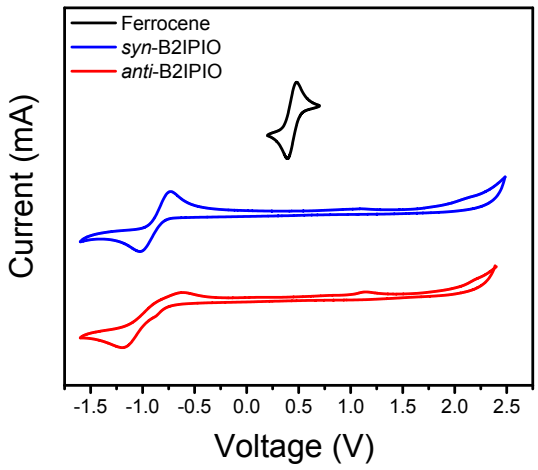

Figure S3. Cyclic voltammograms of *syn*-B2IPIO and *anti*-B2IPIO. Cyclic voltammogram of the two compounds measured with a scan rate of 100 mV s^{-1}.

4. Thermal Properties

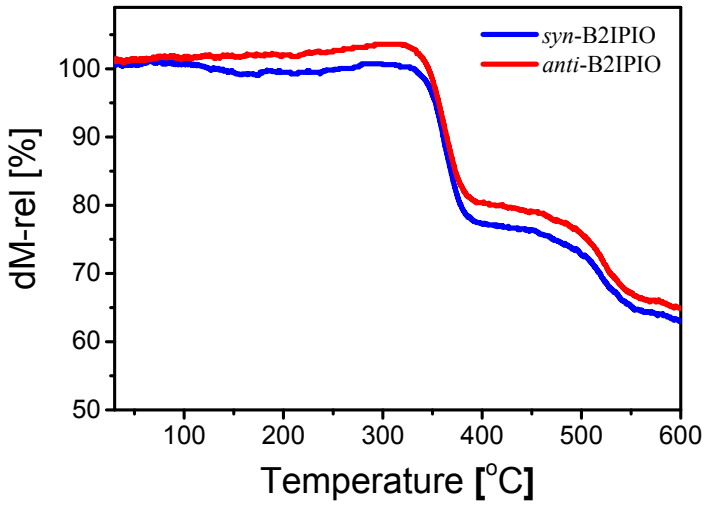

Figure S4. Thermal Gravimetric Analysis (TGA) for *syn*-B2IPIO and *anti*-B2IPIO.

5. Single-Crystal X-ray Analysis

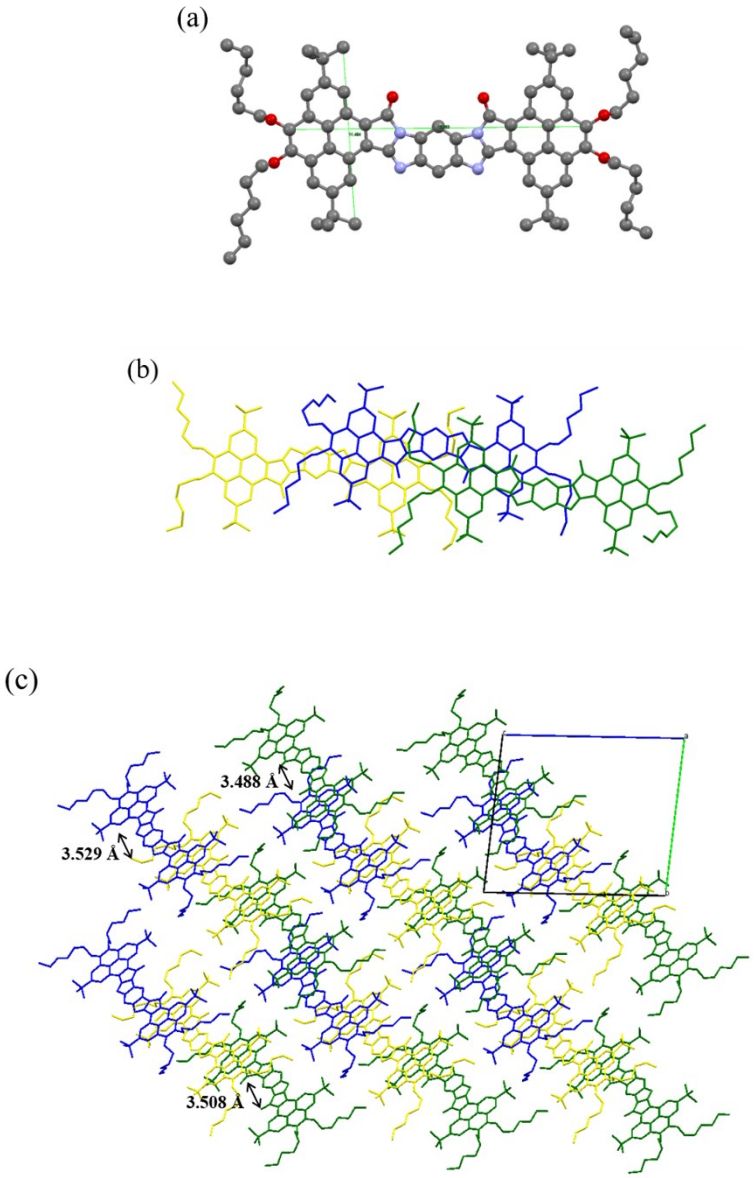

Figure S5. a) Single-crystal structure, b) top view, and c) side view of the crystal packing diagram of *syn*-B2IPIO.

Table S3. Crystal data and structure refinement for *syn*-B2IPIO. (CCDC: 2045205)

Empirical formula	$C_{82}H_{98}N_4O_6$
Formula weight	1235.64
Temperature/K	150.0
Crystal system	triclinic
Space group	P1
a/Å	12.0514(5)
b/Å	19.5147(8)
c/Å	22.9546(9)
α/°	83.729(2)
β/°	76.635(2)
γ/°	87.245(2)
Volume/Å^3	5219.4(4)
Z	3
ρ_{calc}g/cm^3	1.179
μ/mm^{-1}	0.572
F(000)	1998.0
Crystal size/mm^3	0.18 × 0.07 × 0.03
Radiation	CuKα (λ = 1.54178)
2Θ range for data collection/°	4.556 to 122.32
Index ranges	$-13 \leq h \leq 13$, $-22 \leq k \leq 21$, $-26 \leq l \leq 26$
Reflections collected	41888
Independent reflections	27445 [R_{int} = 0.1257, R_{sigma} = 0.0862]
Data/restraints/parameters	27445/57/2543
Goodness-of-fit on F^2	1.015
Final R indexes [I>=2σ (I)]	R_1 = 0.0972, wR_2 = 0.2505
Final R indexes [all data]	R_1 = 0.1327, wR_2 = 0.2982
Largest diff. peak/hole / e Å^{-3}	0.65/-0.31
Flack parameter	-0.1(4)

6. Characterization of Nonvolatile OFET Memory Devices

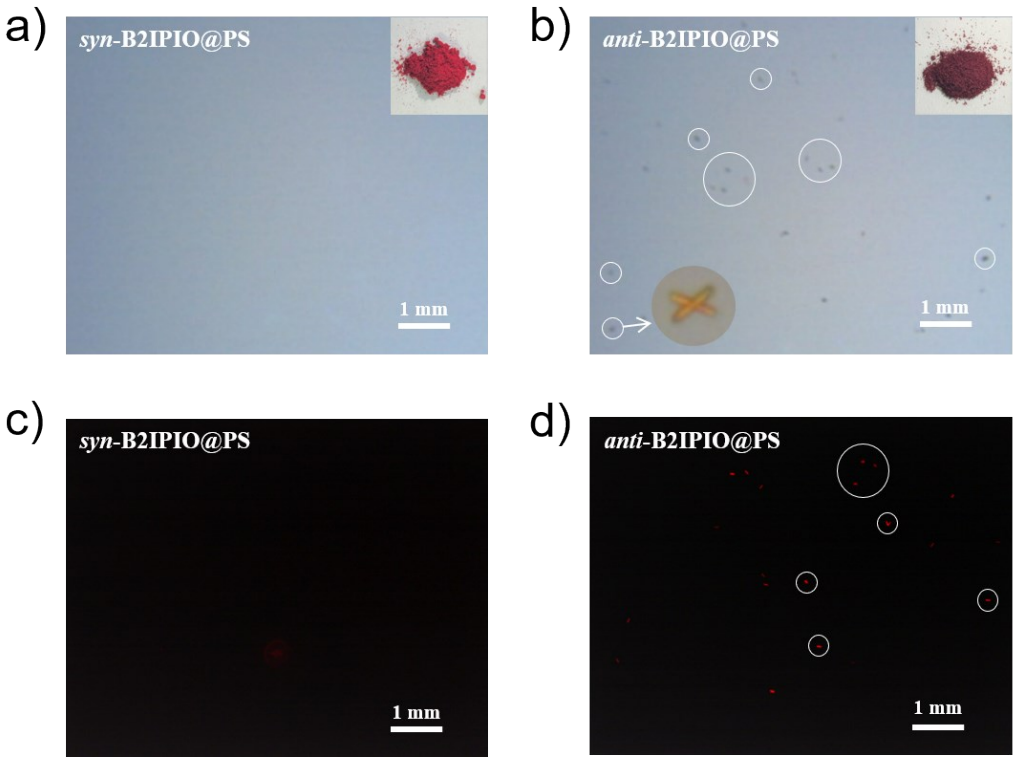

Figure S6. Optical images of a) *syn*-B2IPIO@PS and b) *anti*-B2IPIO@PS blend films, and c) *syn*-B2IPIO@PS and d) *anti*-B2IPIO@PS under bright field (ortho) microscope.

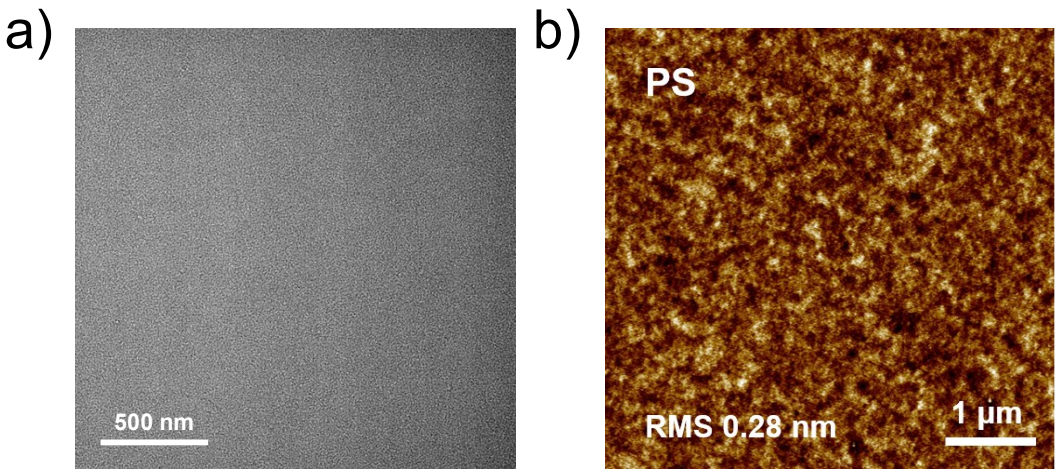

Figure S7. a) TEM image of pure PS film, and b) AFM topographic images of pure PS film on SiO_2/Si substrates, on 5 μm × 5 μm areas.

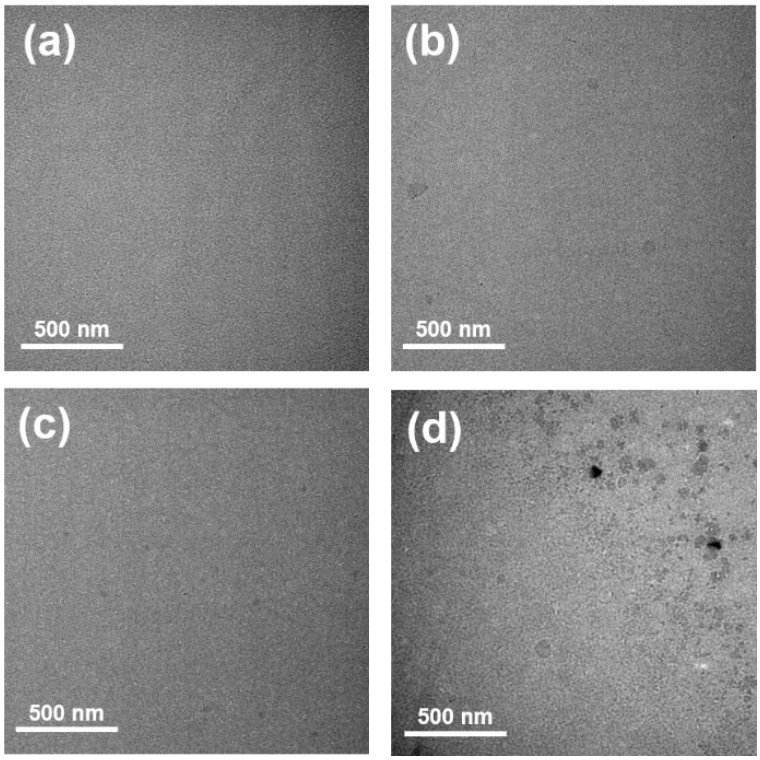

Figure S8. TEM images of the a) 0.5%*syn*-B2IPIO@PS, b) 3%*syn*-B2IPIO@PS, c) 0.5%*anti*-B2IPIO@PS and d) 3%*anti*-B2IPIO@PS blend films.

We have tested the X-ray diffraction (XRD) of *syn*-B2IPIO and *anti*-B2IPIO powders and films, respectively. Both *syn*-B2IPIO and *anti*-B2IPIO powders showed sharp diffraction peaks. However, the film of *syn*-B2IPIO did not show any diffraction peaks, indicating its amorphous state in the film state.[22] In contrast, the XRD of *anti*-B2IPIO film shows (001) diffraction peak around $2\theta = 6$ °, suggesting significant aggregation and crystallization of *anti*-B2IPIO in thin film.

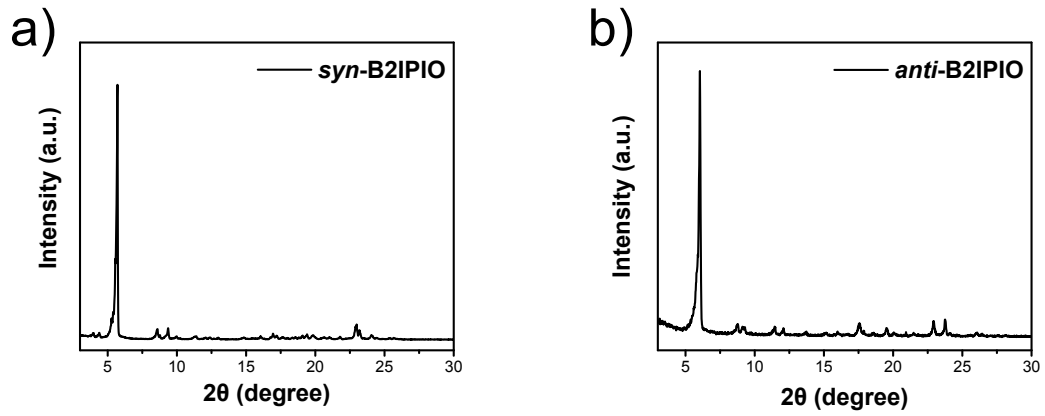

Figure S9. X-ray diffraction from the powder of *syn*-B2IPIO and *anti*-B2IPIO.

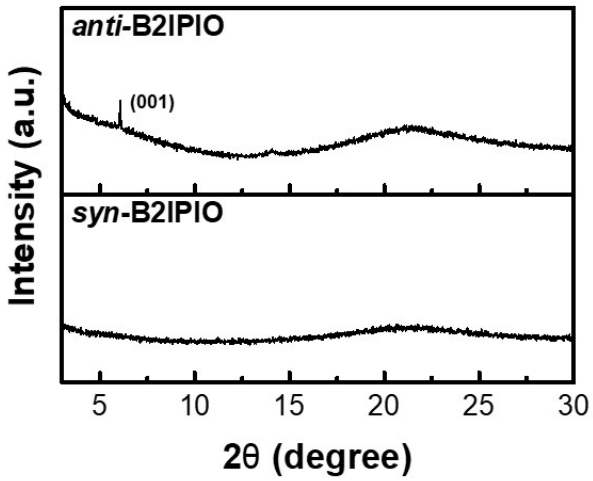

Figure S10. X-ray diffraction from the films of *syn*-B2IPIO and *anti*-B2IPIO on SiO_2 dielectrics.

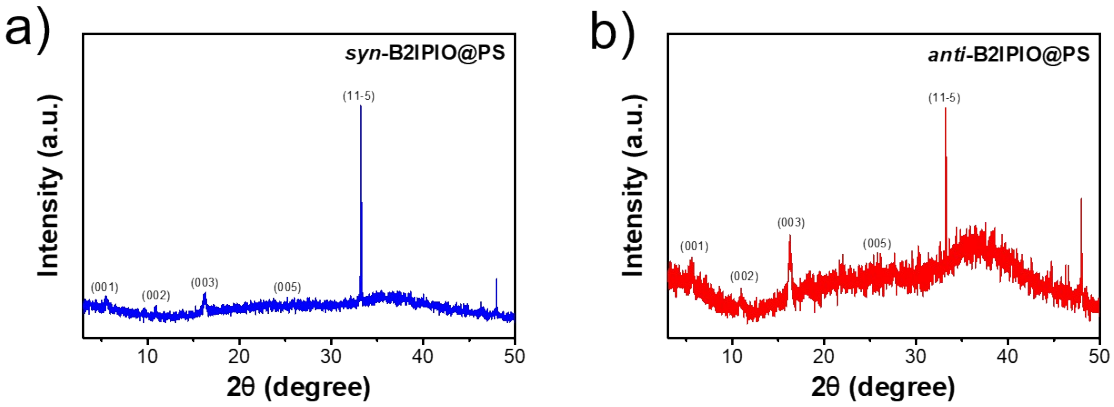

Figure S11. XRD of TIPS-pentacene deposited on a) *syn*-B2IPIO@PS blend film and b) *anti*-B2IPIO@PS blend film.

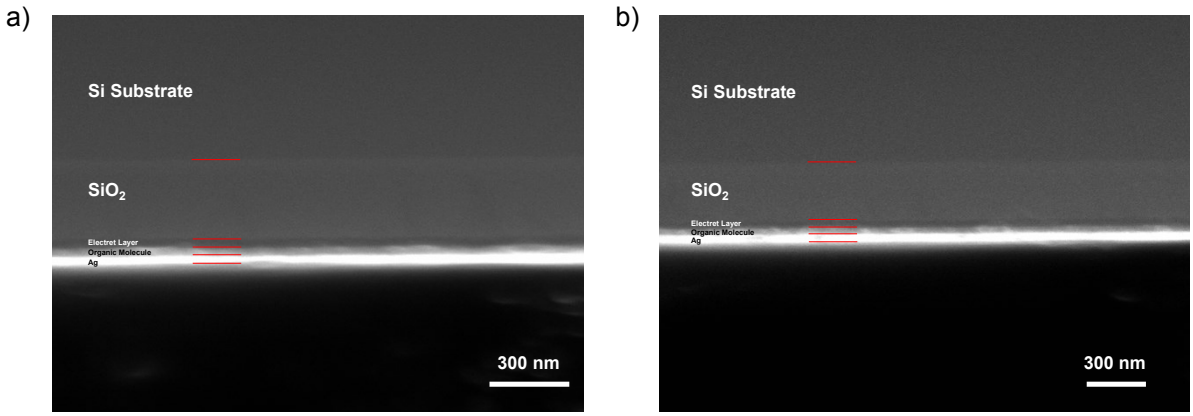

Figure S12. Cross-section scanning electron microscope (SEM) images of the memory devices with a) *syn*-B2IPIO@PS blend film and b) *anti*-B2IPIO@PS blend film as electret layer.

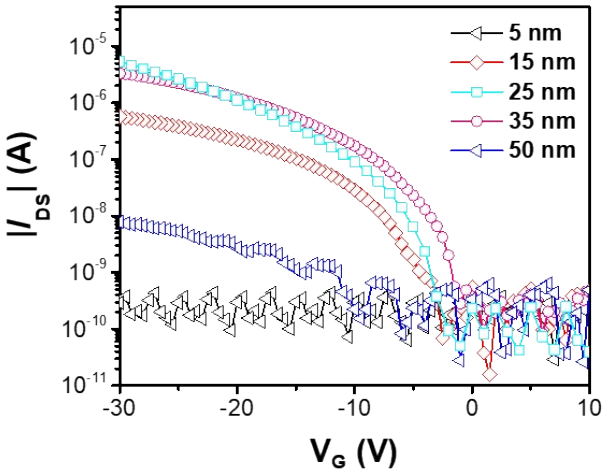

Figure S13. Transfer curve of TIPS-pentacene of different thickness deposited on PS films.

Table S4. Transistor performances of TIPS-pentacene with different thicknesses.

Thickness [nm]	μ [$cm^2V^{-1}s^{-1}$]	V_{th} [V]	I_{ON}/I_{OFF}
5	-	-	-
15	1.02×10^{-2} (8.04×10^{-3})	-2.7 (-3.4)	10^4
25	8.00×10^{-2} (7.37×10^{-2})	-1.5 (-3.7)	10^5
35	3.35×10^{-2} (2.69×10^{-2})	-1.6 (-3.0)	10^5
50	1.10×10^{-4} (9.60×10^{-5})	-7.2 (-9.8)	10^2

We have tested the carrier mobility of devices with different thicknesses of TIPS-pentacene vapor-deposited on the pure PS layer. It is found that when the thickness of TIPS-pentacene is 25 nm, the device has the best hole mobility.

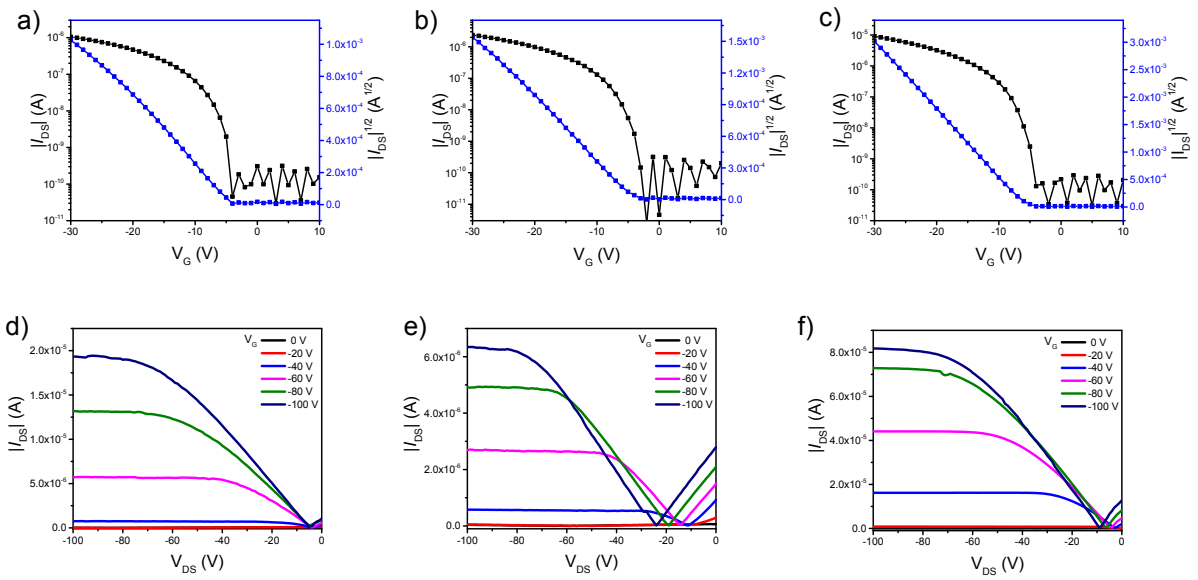

Figure S14. transfer and output characteristic curves of memory devices with a), d) PS film, b), e) *syn*-B2IPIO@PS blend film and c), f) *anti*-B2IPIO@PS as electret layer.

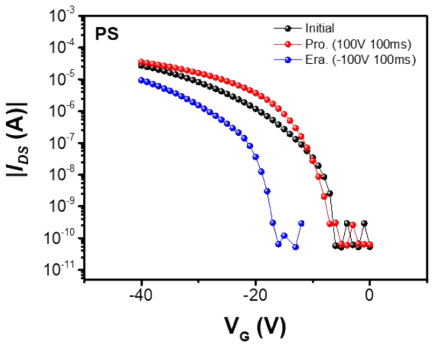

Figure S15. Transfer characteristic curves of memory devices with PS film.

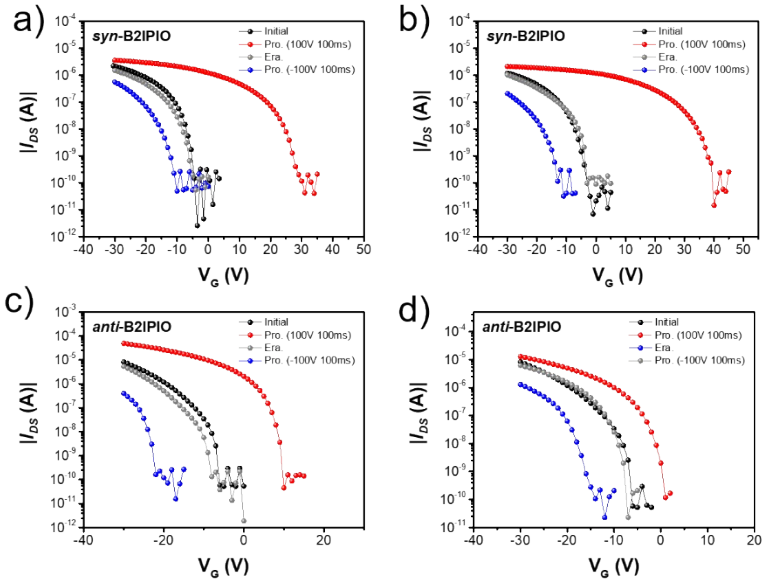

Figure S16. Transfer characteristic curves of memory devices with a) 0.5%*syn*-B2IPIO@PS, b) 3%*syn*-B2IPIO@PS, c) 0.5%*anti*-B2IPIO@PS and d) 3%*anti*-B2IPIO@PS blending films as electret layer.

Table S5. Transistor and memory performances of OFET memory devices.

Compounds	μ [$cm^2 V^{-1} s^{-1}$]	V_{th} [V]	Memory window [V]	Δn [$10^{12} cm^{-2}$]
pure PS	0.080 (0.074)	-1.6 (-3.0)	14.8 (11.2)	0.75 (0.57)
0.5%*syn*-B2IPIO@PS	0.067 (0.048)	-1.7 (-3.1)	43.1 (41.3)	2.58 (2.46)
3%*syn*-B2IPIO@PS	0.044 (0.037)	-1.3 (-3.5)	53.2 (50.9)	3.17 (3.04)
0.5%*anti*-B2IPIO@PS	0.059 (0.050)	-4.7 (-6.1)	21.8 (20.3)	1.82 (1.69)
3%*anti*-B2IPIO@PS	0.061 (0.041)	-5.3 (-7.0)	17.8 (14.4)	1.48 (1.20)

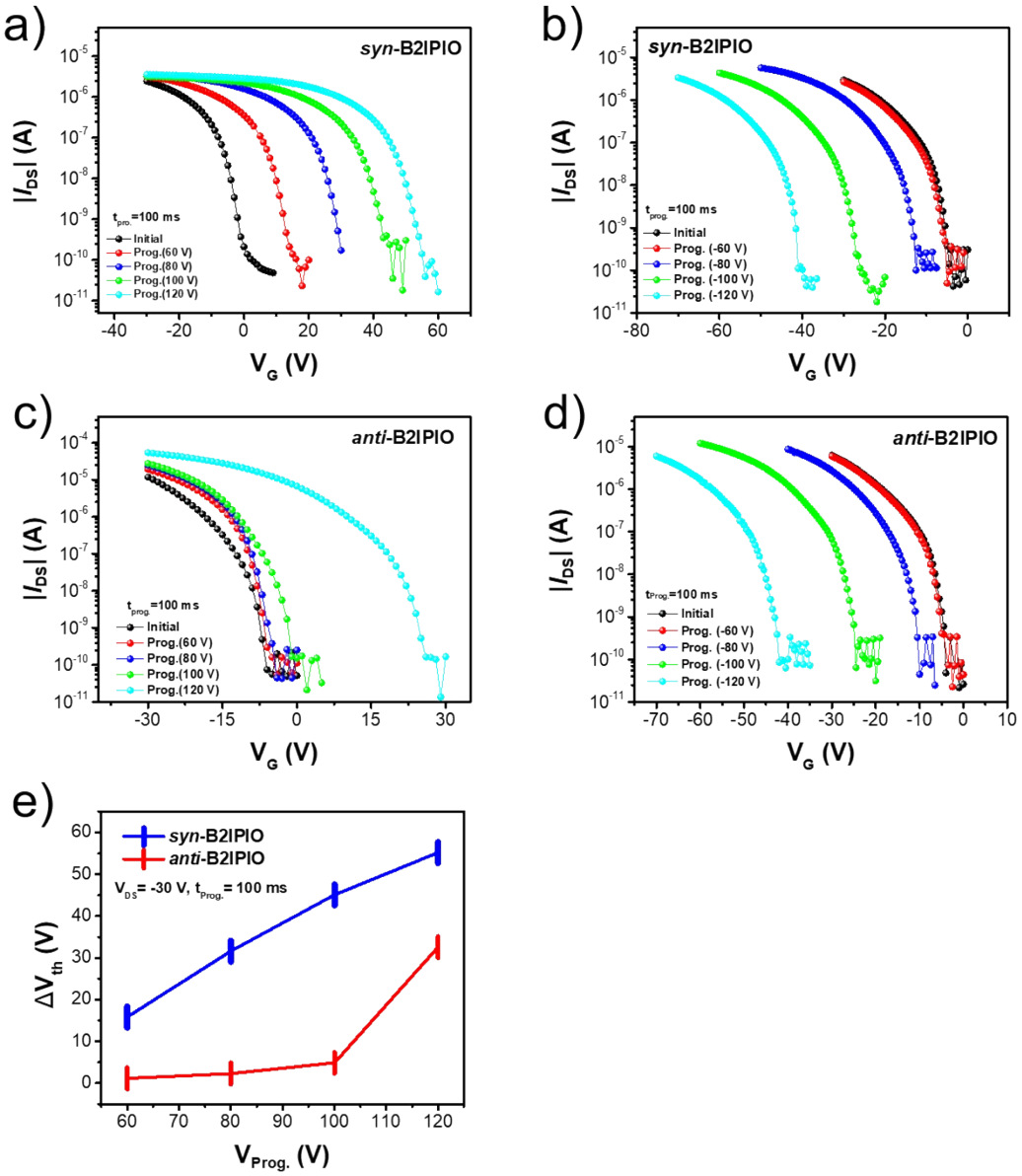

Figure S17. The transfer curves of the a) *syn*-B2IPIO@PS, c) *anti*-B2IPIO@PS based memory devices for the programming processes under positive gate voltages ranging from 60, 80, 100 to 120 V. The drain current was measured at V_{DS} = -30 V and the programming time was 100 ms, b) *syn*-B2IPIO@PS, d) *anti*-B2IPIO@PS based devices for the negative programming processes upon negative gate voltages ranging from -60, -80, -100 to -120 V, e) shifts of memory windows under different programming voltage.

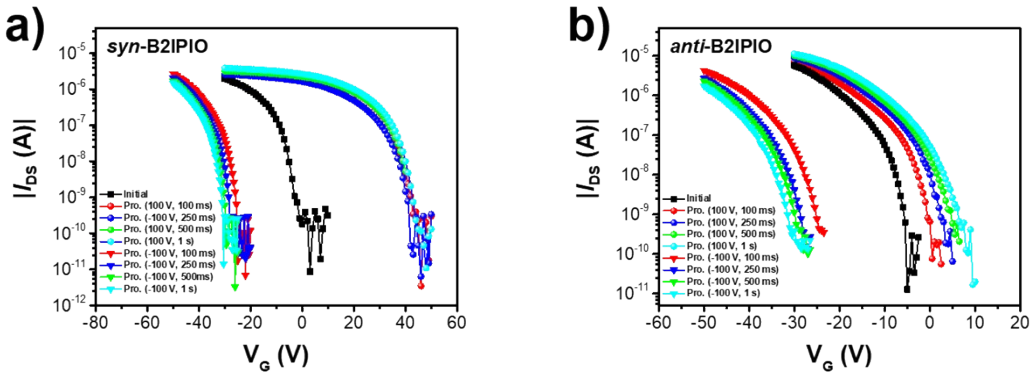

Figure S18. The transfer characteristics of a) *syn*-B2IPIO@PS and b) *anti*-B2IPIO@PS based OFET memory devices. The programming time was changing from 100 ms to 1 s under ±100 V gate voltage.

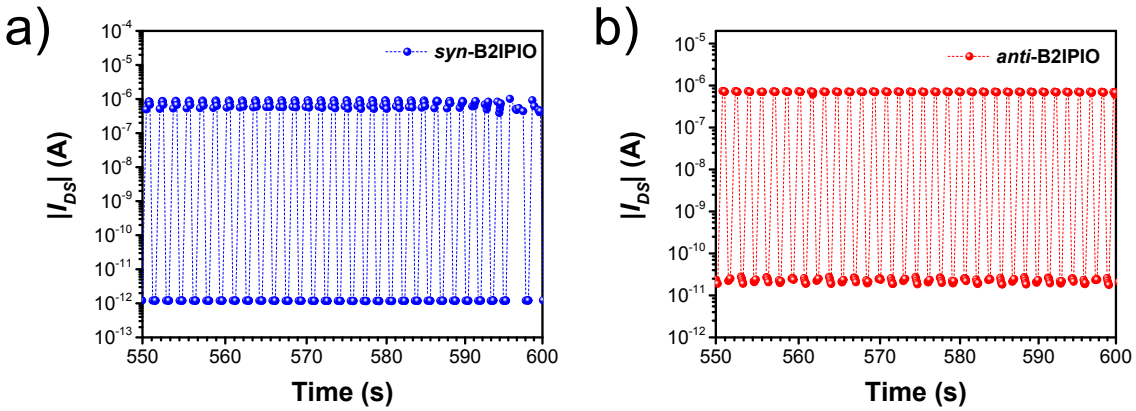

Figure. S19. Write-read-erase-read (WRER) cycles testing of a) *syn*-B2IPIO@PS and b) *anti*-B2IPIO@PS based OFET memory devices.

Table S6. Comparison of key operating parameters of OFET-based memory devices from the literature.

Channel material	Dielectric material	Charge storage element	Operating voltage (V_{OP})	Memory window ΔV_{th} (V)	Ref.
C_8-BTBT	PMMA	P(VDF-TrFE)	± 15	12	33
C_{60}	Al_2O_3	diarylethene **1o**	3 to -10	10	34
F8T2	PS	Au NPs	± 90	30	35
Pentacene	Al_2O_3	ZnTe	±15	10	36
Pentacene	SiO_2/300 nm	P13	±120	60	2
Pentacene	SiO_2/300 nm	$TPA(PDAF)_3$	±100	89	15
Pentacene	PVA	Au NP	± 90	10	37
TIPS-pentacene	PS	IPPA-Cl	± 80	40.8	14
$N(PTPMA)_3$: TIPS-pentacene	SiO_2/300 nm	PS Brush	-120 to 100	55	38
TIPS-pentacene	PS	*syn*-B2IPIO	±100	59.2	This work
TIPS-pentacene	PS	*anti*-B3IPIO	±100	25.5	

7. ^{1}H NMR and ^{13}C NMR Spectra

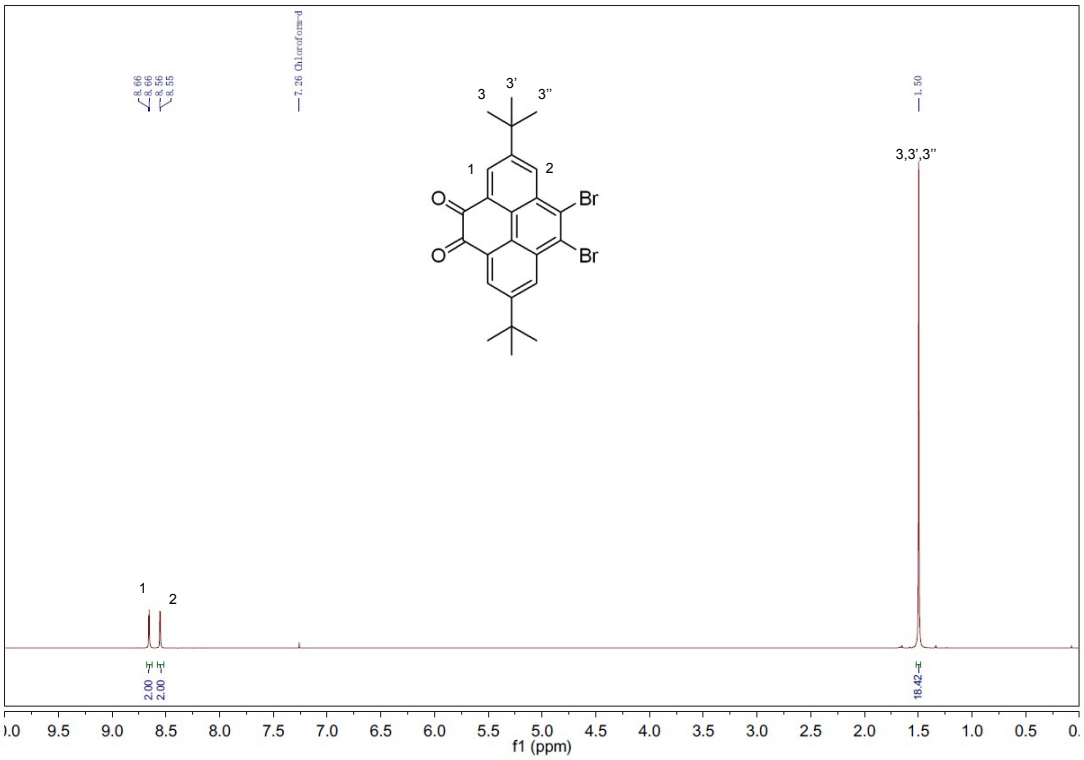

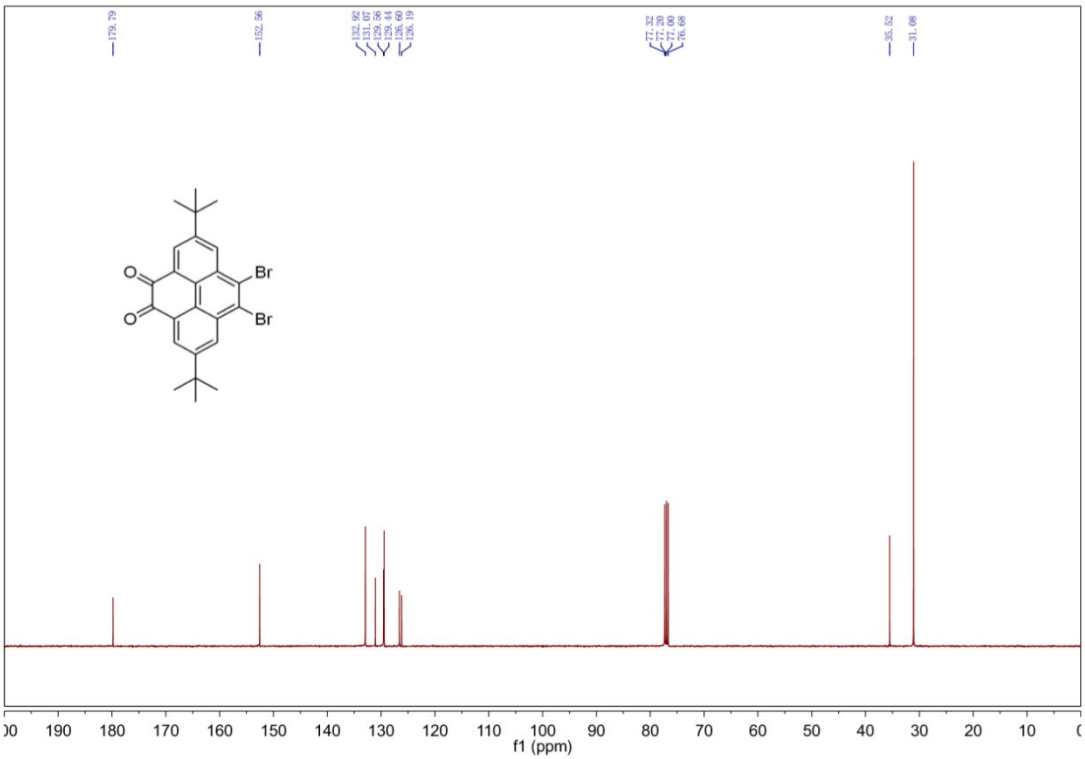

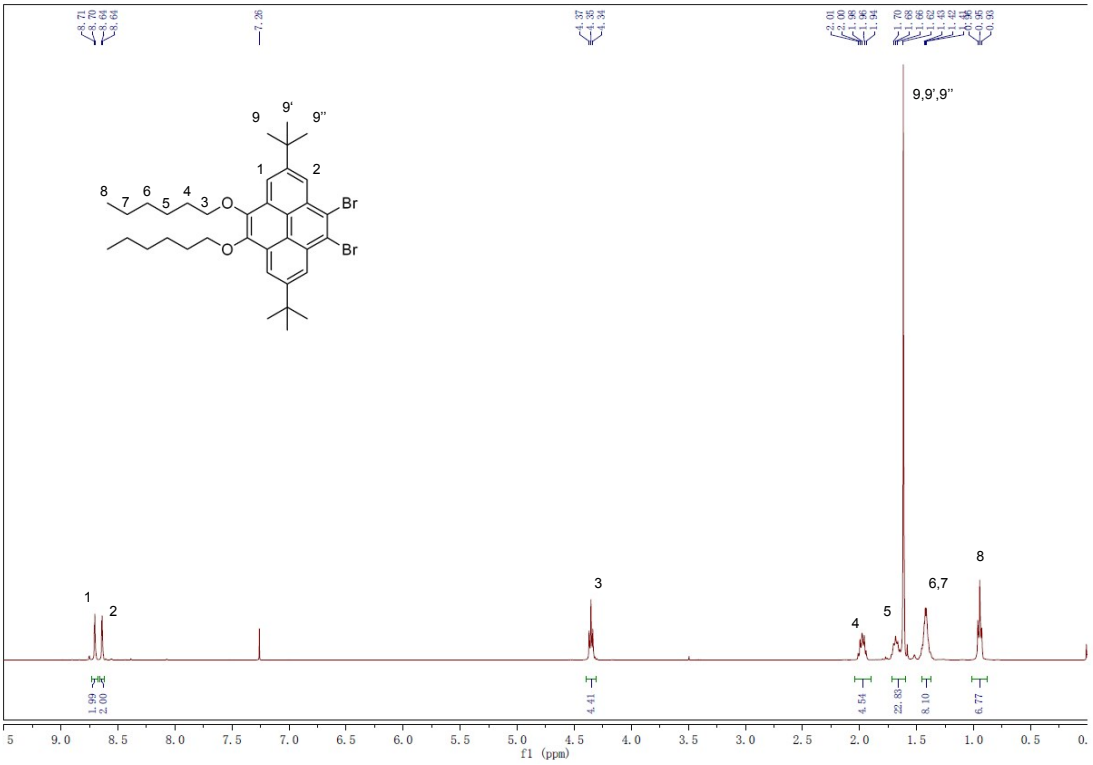
9
9'
9''
1
2
8
7
6
5
4
3
O
O
Br
Br
9,9',9''
1
2
3
4
5
6,7
8
f1 (ppm)

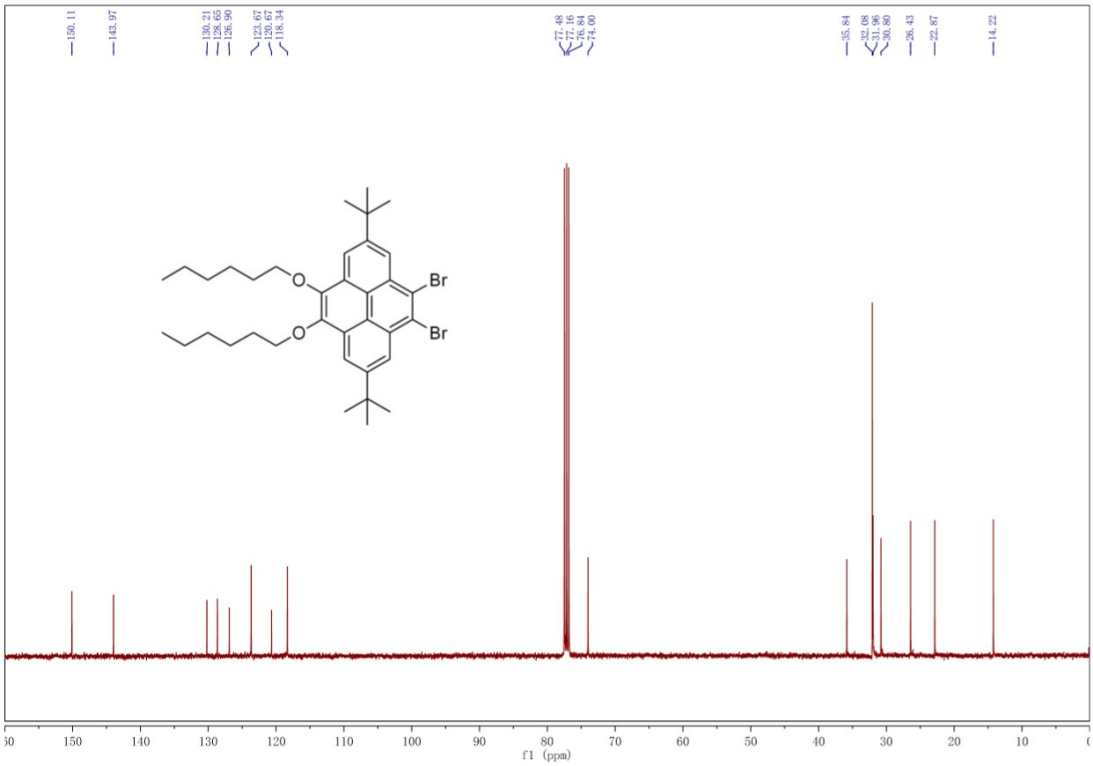
Br
Br
O
O
f1 (ppm)

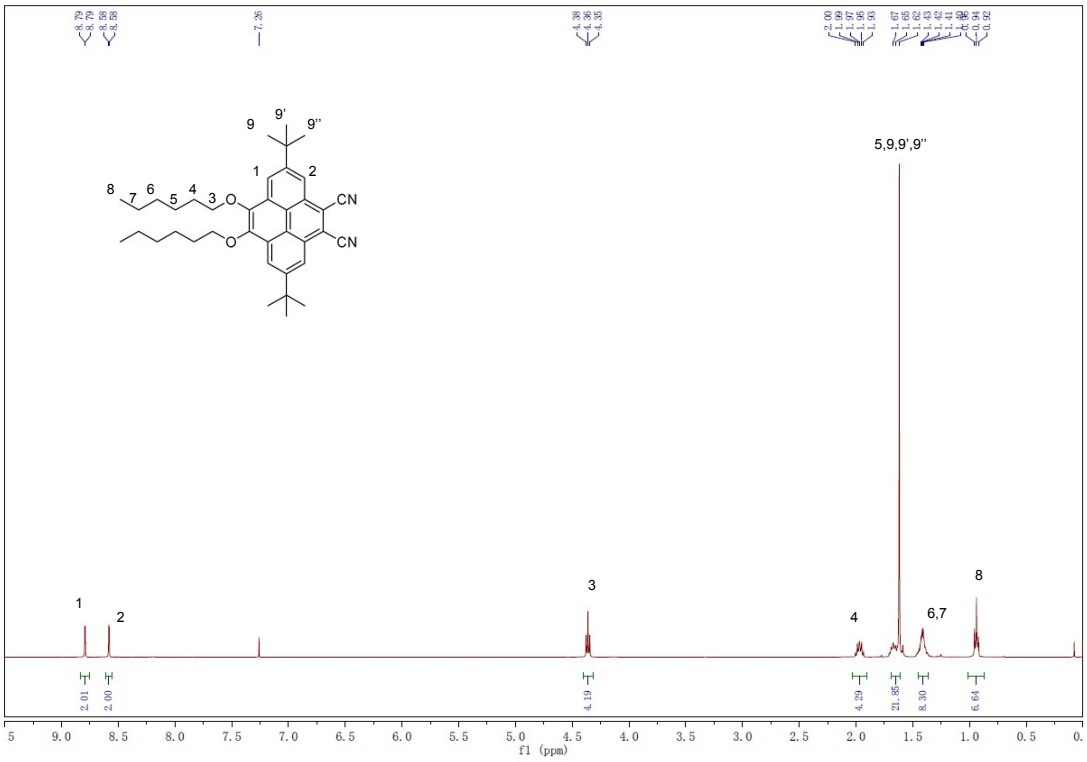
9
9'
9''
1
2
8
7
6
5
4
3
O
O
CN
CN
5,9,9',9''
1
2
3
4
6,7
8
2.01
2.00
4.19
4.29
21.85
8.30
6.64
f1 (ppm)

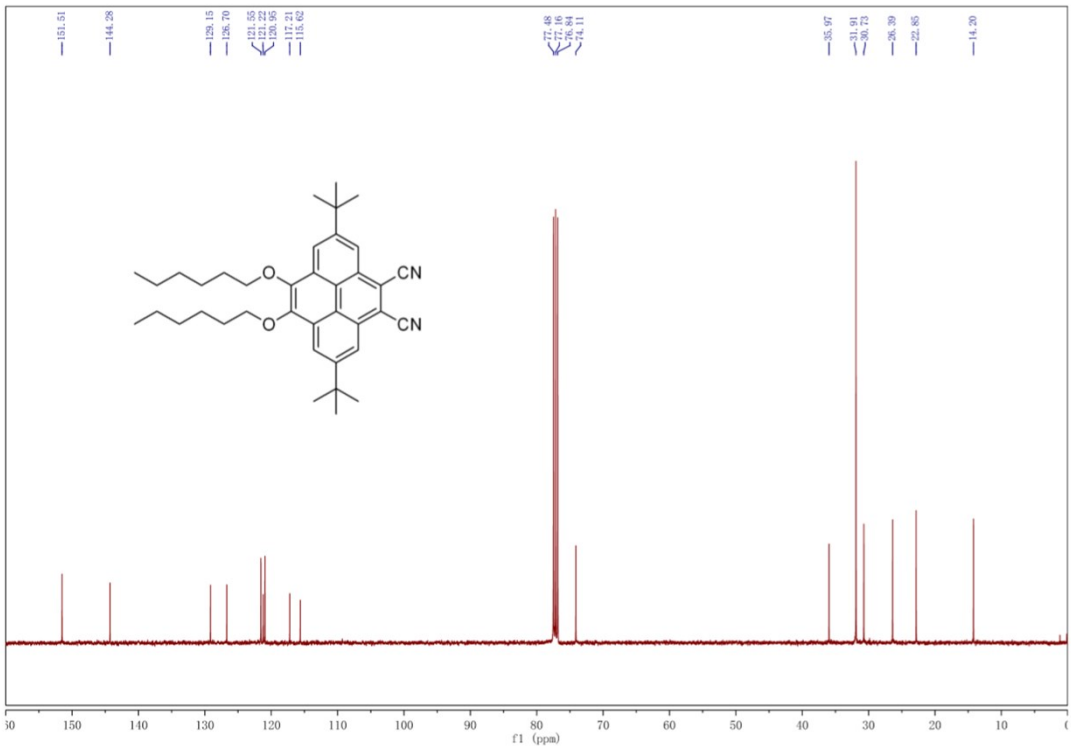
O
O
CN
CN
f1 (ppm)

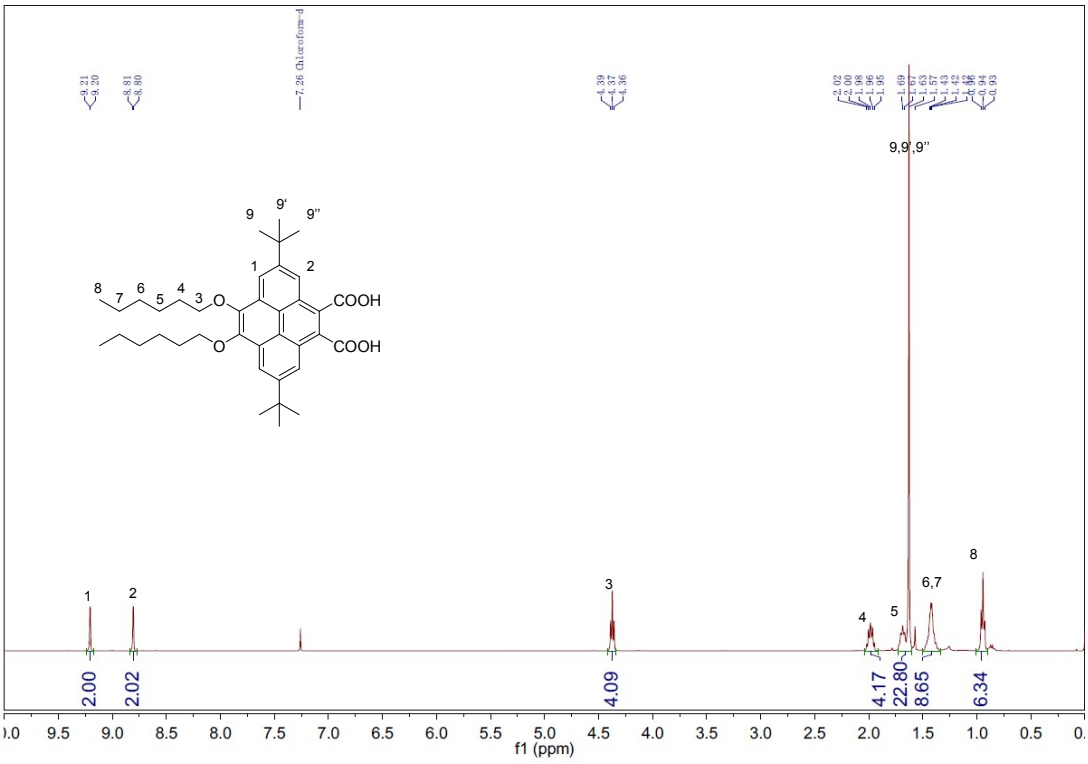
9,9',9''
1
2
3
4
5
6,7
8
2.00
2.02
4.09
4.17
22.80
8.65
6.34
COOH
COOH
f1 (ppm)

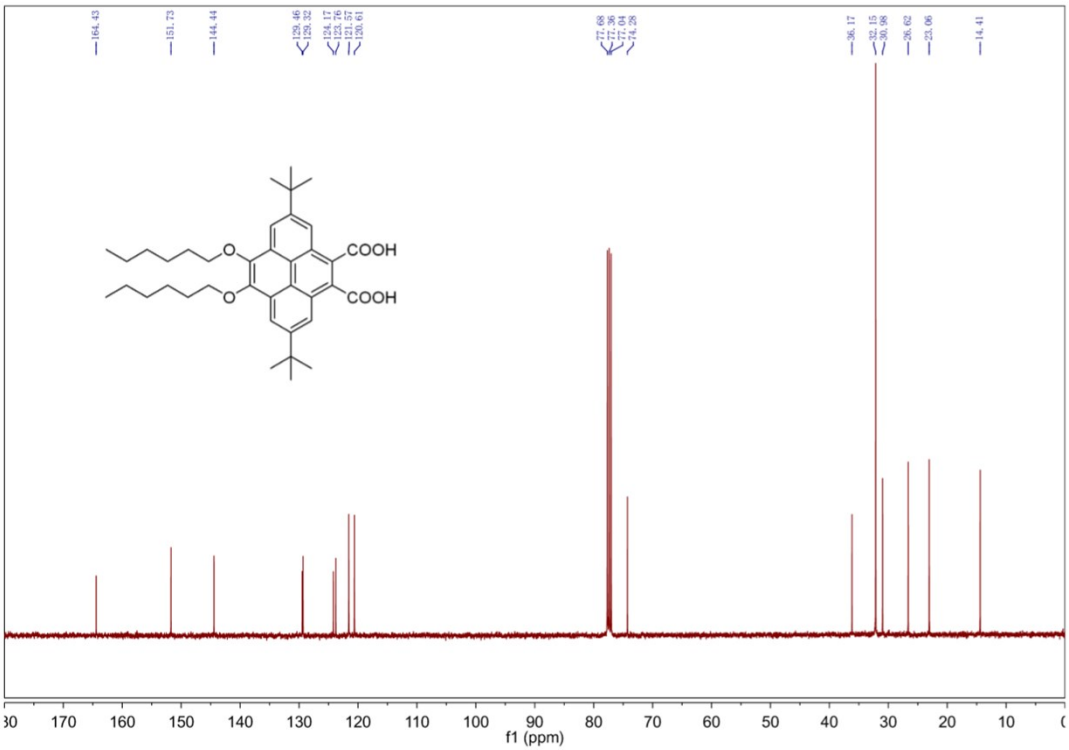
COOH
COOH
f1 (ppm)

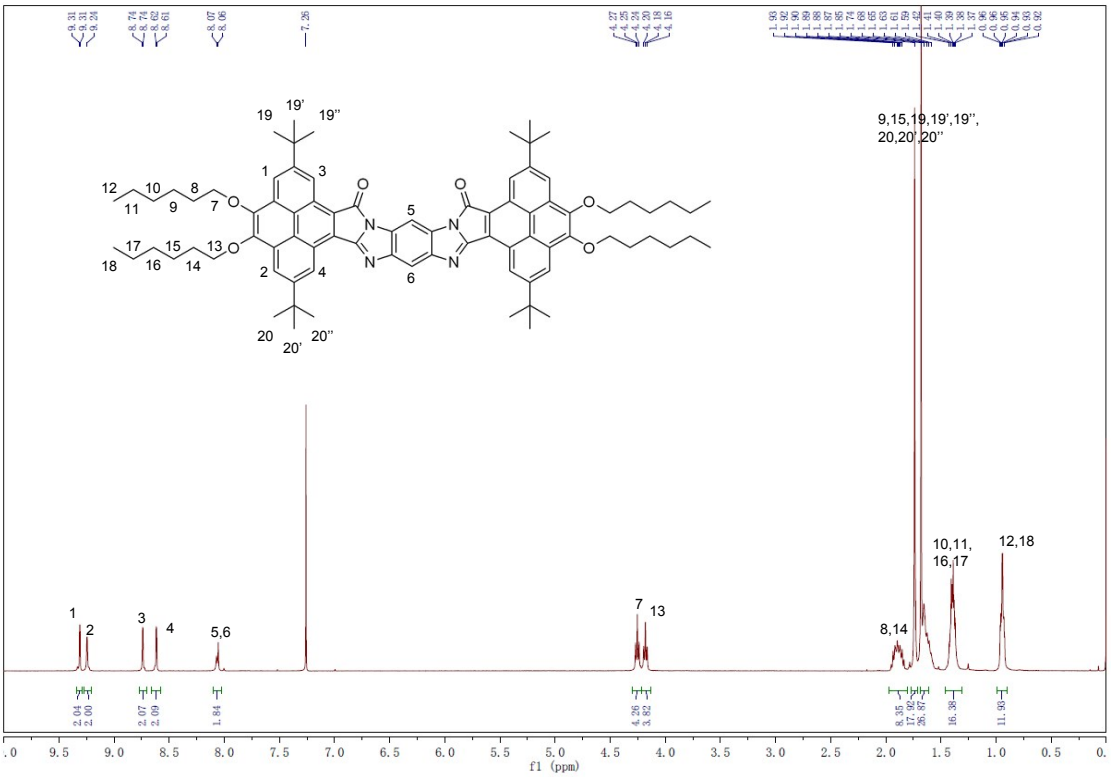
9,15,19,19',19'',
20,20',20''
10,11,
16,17
12,18
8,14
7
13
1
2
3
4
5,6
f1 (ppm)

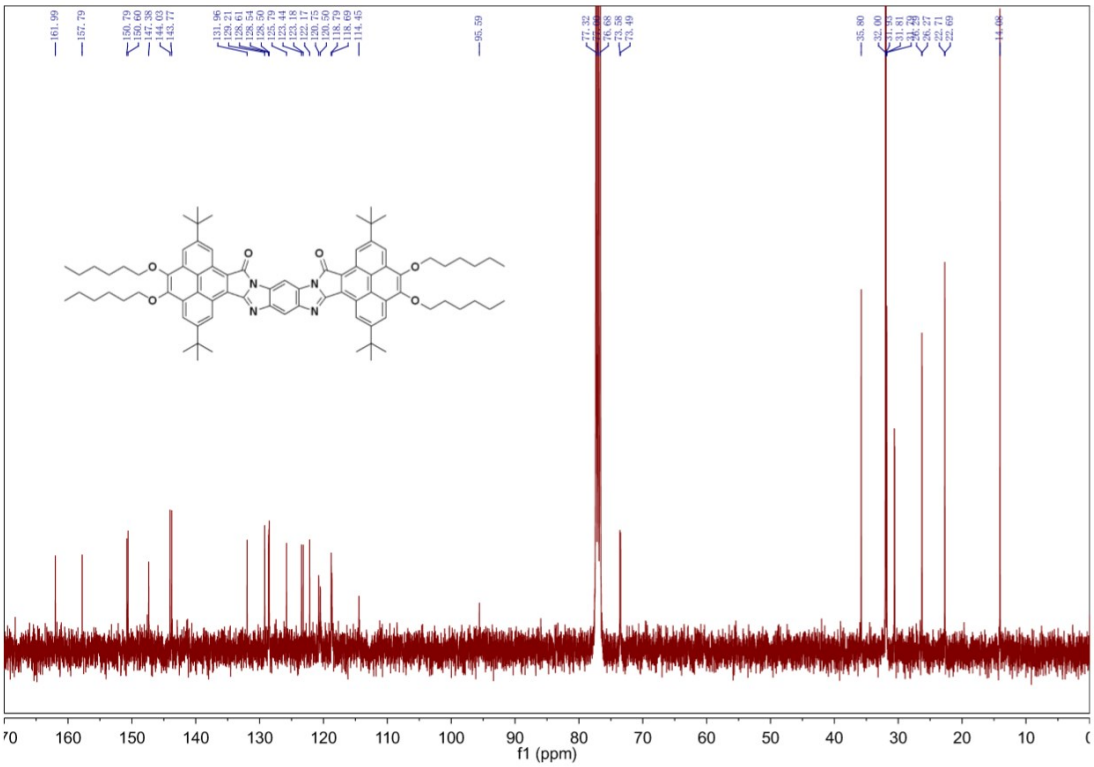
f1 (ppm)

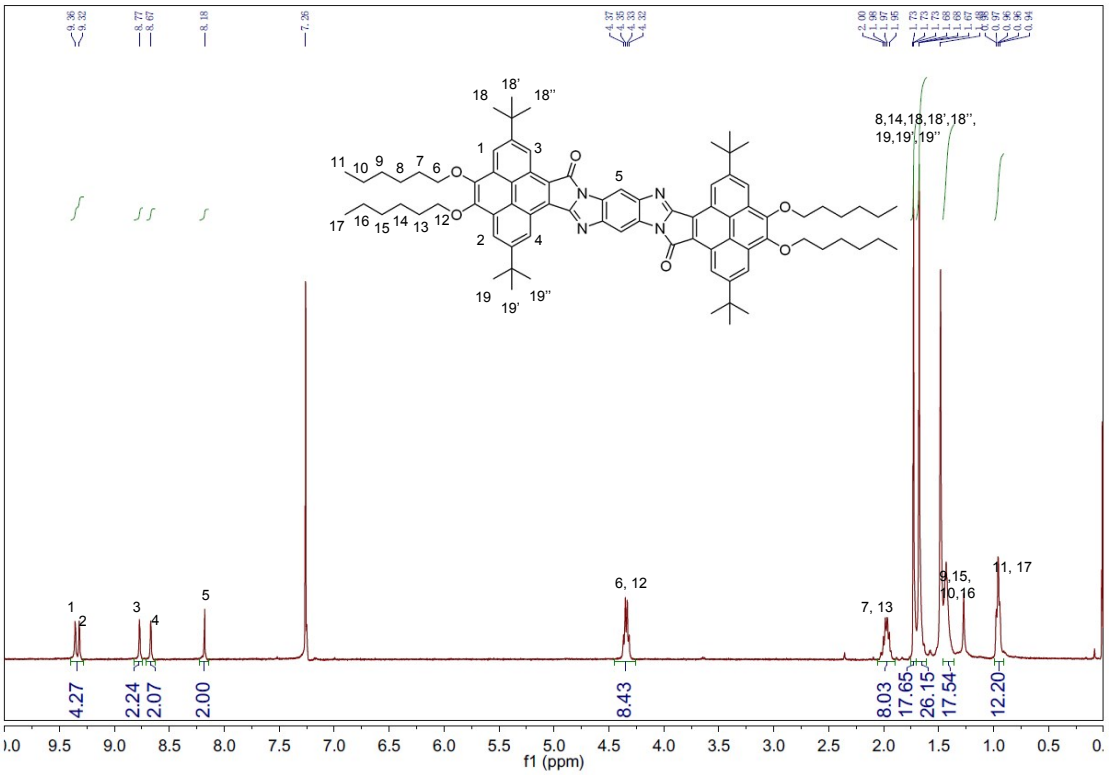

8. HRMS Spectra

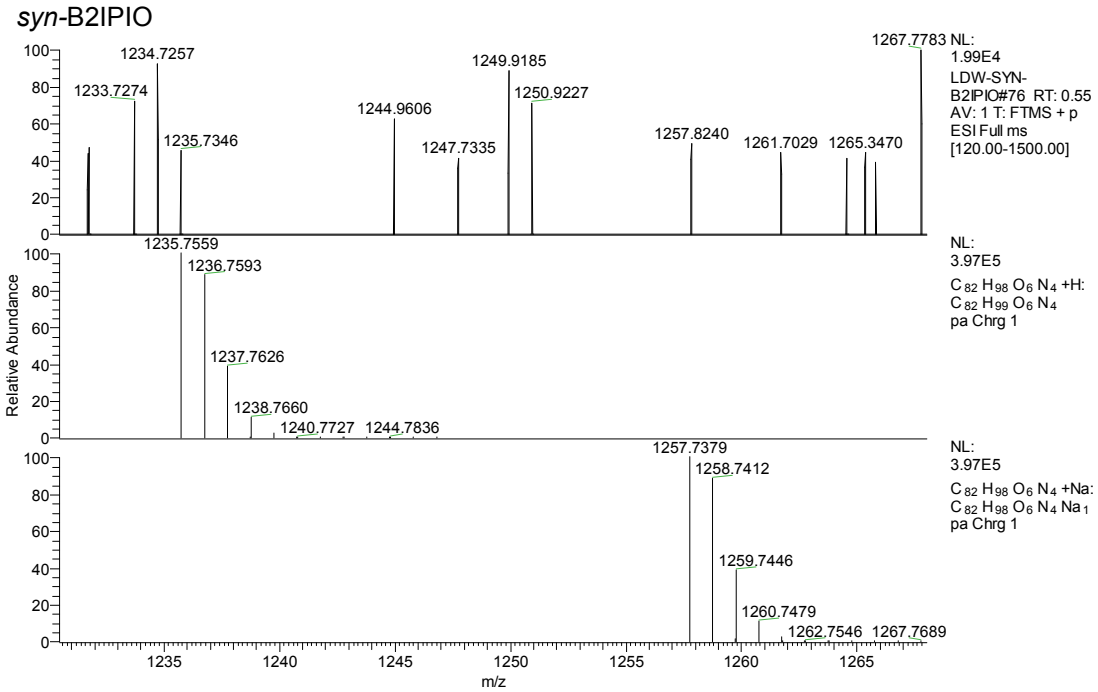

anti-B2IPIO

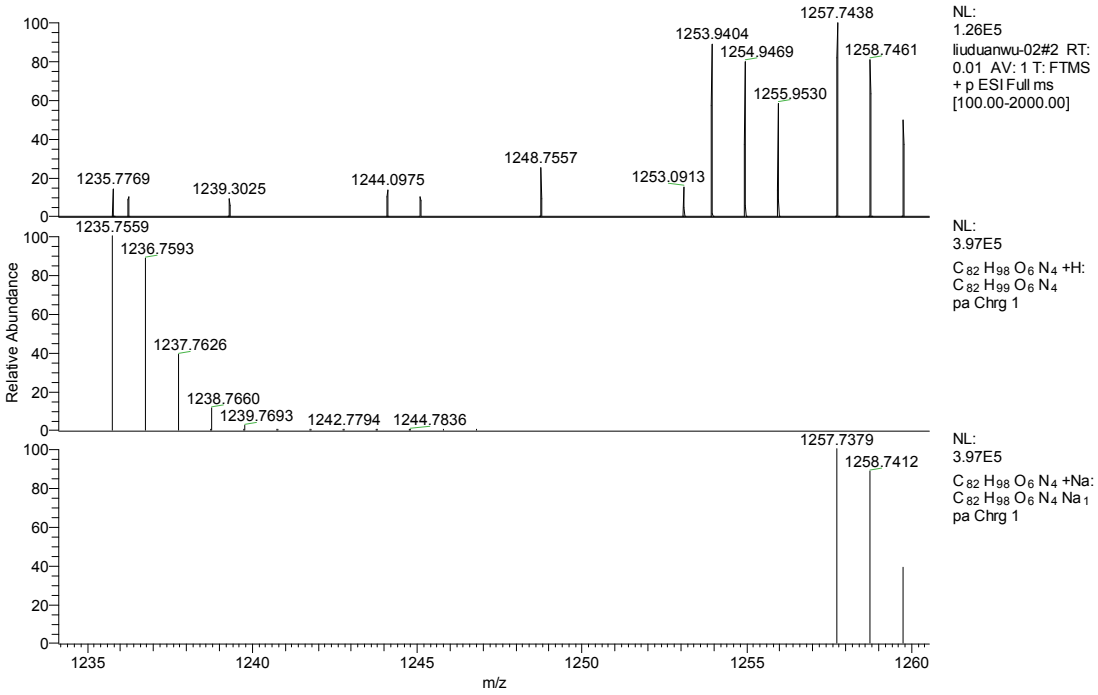
1257.7438
1253.9404
1254.9469
1258.7461
1255.9530
1248.7557
1235.7769
1239.3025
1244.0975
1253.0913
NL:
1.26E5
liuduanwu-02#2 RT:
0.01 AV: 1 T: FTMS
+ p ESI Full ms
[100.00-2000.00]
1235.7559
1236.7593
1237.7626
1238.7660
1239.7693
1242.7794
1244.7836
NL:
3.97E5
C82 H98 O6 N4 +H:
C82 H99 O6 N4
pa Chrg 1
1257.7379
1258.7412
NL:
3.97E5
C82 H98 O6 N4 +Na:
C82 H98 O6 N4 Na1
pa Chrg 1
Relative Abundance
m/z
1235
1240
1245
1250
1255
1260